Talanta 280 (2024) 126750

Contents lists available at ScienceDirect

Talanta

journal homepage: www.elsevier.com/locate/talanta

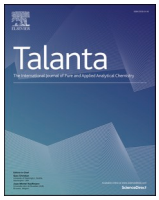

Pancreatic lipase immobilization on cellulose filter paper for inhibitors screening and network pharmacology study of anti-obesity mechanism

Guangxuan Chen [a], Huicong Yuan [a], Lumei Zhang [a], Jingran Zhang [b], Kefeng Li [c,**], Xu Wang [a,*]

[a] State Key Laboratory of Food Nutrition and Safety, College of Food Science and Engineering, Tianjin University of Science and Technology, Tianjin, 300457, China
[b] SCIEX, Analytical Instrument Trading Co., Ltd, Beijing, 100015, China
[c] Centre for Artificial Intelligence Driven Drug Discovery, Faculty of Applied Sciences, Macao Polytechnic University, Macao SAR, China

ARTICLE INFO

Keywords:
Pancreatic lipase
Immobilized enzyme
Natural products
Inhibitor screening
Black tea
Network pharmacology

ABSTRACT

The discovery of pancreatic lipase (PL) inhibitors is an essential route to develop new anti-obesity drugs. In this experiment, chitosan was used to add amino groups to cellulose filter paper (CFP) and then glutaraldehyde was used to covalently combine PL with amino-modified CFP through the Schiff base reaction. Under optimal immobilization conditions, CFP immobilized PL has a wide range of pH and temperature tolerance, as well as excellent reproducibility, reusability and storage stability. Subsequently, 26 natural products (NPs) were screened by immobilized PL with black tea extract having the highest inhibition rate. Three compounds with binding effects on PL (epigallocatechin gallate, theaflavin-3-gallate and theaflavin-3,3′-digallate) were captured. Molecular docking proved that these three compounds have a strong binding affinity for PL. Fluorescence spectra further revealed that theaflavin-3,3′-digallate could statically quench the intrinsic fluorescence of pancreatic lipase. The molecular docking and thermodynamic parameters indicated that electrostatic interaction was considered as the main interaction force between PL and theaflavin-3,3′-digallate. Finally, the potential anti-obesity targets and pathways of the three compounds were discussed through network pharmacology. This study not only proposes a simple and efficient method for screening PL inhibitors, but also sheds light on the anti-obesity mechanism of active compounds in black tea.

1. Introduction

In this century, obesity has emerged as one of the biggest risks to human health, with approximately 3.40 million adults dying from obesity per year [1]. Obesity may also give rise to hyperlipidemia, hypertension, type 2 diabetes, arteriosclerosis and other connected disorders [2]. Excessive consumption of high-energy and high-fat diets is major factor leading to obesity. Foodborne lipids can be hydrolyzed to absorbable monoglycerides and fatty acids by PL released from the pancreas [3]. Consequently, inhibition of PL to reduce lipid adsorption is a promising method for the treatment of obesity [4]. Orlistat is an effective and specific PL inhibitor, but long-term use can cause serious gastrointestinal side effects [5]. Thus, the development of effective PL inhibitors with low side effects as anti-obesity drugs is urgently needed.

As we all know, natural products have a significant number of bioactive compounds, making them one of the primary sources for new drug development. In terms of practical application, NPs have fewer side effects and better biocompatibility than other medicines [6]. Furthermore, NPs, due to their structural variety, can concurrently regulate several targets, involve various mechanisms of action, and take part in the feedback interactions of numerous links in the illness network [7]. As a result, it is of great significance to screen lipase inhibitors from NPs and explore their anti-obesity mechanism.

As a screening technique based on molecular targeting strategies, immobilized enzyme has the advantages of tolerance to changes in temperature and pH, as well as good reproducibility, reusability and stability [8]. However, the carrier and immobilization technique are the most important factors to consider. As a new type of immobilized enzyme carrier, CFP is distinguished by wide source, low cost, large surface, rich surface hydroxyl groups and easy modification [9]. Most importantly, it did not require the time-consuming separation required for other carriers like magnetic nanoparticles and nanomaterials,

* Corresponding author. State Key Laboratory of Food Nutrition and Safety, College of Food Science and Engineering, Tianjin University of Science and Technology, Tianjin 300457, China.
** Corresponding author.
E-mail addresses: kefengl@mpu.edu.mo (K. Li), xuwang@tust.edu.cn (X. Wang).

https://doi.org/10.1016/j.talanta.2024.126750
Received 18 May 2024; Received in revised form 8 July 2024; Accepted 21 August 2024
Available online 23 August 2024

allowing it to be removed straight from the reaction solution [10]. For subsequent enzyme immobilization, functional groups were used to modify CFP to form enzyme binding sites. Due to its good biocompatibility and biodegradability, as well as moderate viscosity, chitosan (CS) is an ideal modifier. It is possible to add amino groups to the surface of CFP, which facilitates the further immobilization of enzymes. The enzyme was then covalently bound to amino-functionalized CFP through the Schiff base reaction using glutaraldehyde (GA) as a cross-linking agent.

In this study, the immobilized conditions of CFP immobilized PL were optimized and its performance was evaluated. The enzymatic kinetics and inhibition kinetics of immobilized PL, as well as the inhibitory effects of 26 NPs on immobilized PL was explored. The active compounds in black tea extract were subsequently captured with CFP immobilized PL and identified by ultra-high performance liquid chromatography quadrupole time-of-flight tandem mass spectrometry (UHPLC-QTOF-MS/MS), and their potential interactions with PL were determined by molecular docking. Subsequently, molecular docking and fluorescence spectroscopy were utilized to illustrate the mechanism of action of the selected compound with PL. Finally, network pharmacology was utilized to evaluate the anti-obesity mechanisms of the captured active compounds.

2. Materials and methods

2.1. Materials

Pancreatic lipase (PL, 650 U/mg), theaflavin-3,3′-digallate (98 %), glutaraldehyde solution (GA, 50 %) and chitosan (CS, 95 %) were acquired from Sigma-Aldrich (MO, USA). 4-Methylumbelliferyl oleate (4-MUO, 98 %) was purchased from Aladdin Bio-Chem Technology Co., Ltd (Shanghai, China). Orlistat (98 %) was acquired from Macklin Biochemical Co., Ltd (Shanghai, China). Acetic acid, potassium dihydrogen phosphate (KH_2PO_4), hydrochloric acid (HCl) and sodium hydroxide (NaOH) were purchased from Solarbio Technology Co., Ltd (Shanghai, China). HPLC grade dimethyl sulfoxide (DMSO) was purchased from Tianjin Kaixin Chemical Industry Co., Ltd (Tianjin, China). HPLC grade methanol was purchased from Chengdu Kelong Chemical Reagent Factory (Chengdu, China). The medium-speed qualitative cellulose filter paper was acquired from Fushun Civil Affairs Filter Paper Factory (Liaoning, China). All NPs were acquired from Chinese pharmacies.

2.2. Instruments

Black tea extract was analyzed by UHPLC-QTOF-MS/MS system with a Triple TOF 6600 Mass Spectrometer (SCIEX, USA) connected to the ExionLC AD UHPLC system (SCIEX, USA). Agilent ZORBAX C_{18} column (2.1 × 100 mm, 1.8 μm) with solvent A (0.5 % formic acid aqueous solution) and solvent B (acetonitrile) was used for the separation. The gradient program was as follows: 0 min, 10 % B; 4 min, 15 % B; 7 min, 25 % B; 9 min, 32 % B; 16 min, 40 % B; 22 min, 55 % B; 28 min, 95 % B; and 30 min, 95 % B. The flow rate was 0.4 mL/min, the injection volume was 3 μL, and the column temperature was controlled at 40 °C.

The mass spectrometer equipped with an electrospray ionization source (ESI) was operated in negative mode. The conditions for mass spectrometer analysis were set as follows: ion source temperature at 500 °C; ion source gas 1 at 50 psi; ion source gas 2 at 50 psi; curtain gas at 25 psi and ion spray voltage at 4500 V. The mass ranges were set at 50–1000 Da for the TOF-MS scan and 50–1000 Da for the TOF-MS/MS experiments. TOF MS data and MS/MS data were acquired in one injection by information-dependent acquisition (IDA) scan mode with Dynamic Background Subtraction (DBS) enabled.

2.3. Solutions preparation

KH_2PO_4 was dissolved in ultrapure water to prepare a 30 mM phosphate buffer, and HCl or NaOH (1 mol/L) was used to adjust the pH to 5.0–10.0. Stock solutions of 4-MUO and Orlistat were prepared in DMSO with concentrations of 60 mM and 10 mM, stored at −20 °C, and diluted with the phosphate buffer to the required concentrations before use. PL solution is prepared with phosphate buffer before daily use.

Air-dried NPs 2g were ground into powder, and ultrasonic extraction with 40 mL of 70 % ethanol was performed twice. The supernatant obtained after centrifugation was collected and evaporated under reduced pressure in a rotary evaporator until dry. Prior to use, dilute the residues to the desired concentration with phosphate buffer.

2.4. PL immobilization

The method of immobilization of PL is based on previous reports in the literature [11]. Firstly, dissolve 100 mg CS in 10 mL 1 % (v/v) acetic acid solution and let stand until bubbles disappear completely from the solution. After 12 h of immersing the CFP in CS solution, the CFP/CS was rinsed multiple times with ultrapure water until the supernatant approached neutrality. The new CFP was used to absorb the residual liquid from the CFP/CS's surface. Secondly, the CFP/CS was soaked in a 10 % GA solution and oscillated for 5 h at 40 °C on a constant thermostatic oscillator to produce the CFP/CS/GA. It was then cleaned multiple times with ultrapure water, prior to being sucked dry with new CFP. Finally, CFP/CS/GA was submerged in the PL solution (10 mg/mL) and oscillated at 35 °C for 6 h in a constant thermostatic oscillator. The obtained CFP/CS/GA/PL were repeatedly rinsed with phosphate buffer, sucked dry, and then dried at 35 °C in an oven. The dried CFP/CS/GA/PL was made into discs with a diameter of 6 mm using a hole punch and kept at 4 °C for future study.

2.5. Activity measurement of PL

The method of activity measurement of PL is based on previous literature reports with slight modifications [12]. In the PL catalyzed reaction, 4-MUO was used as the substrate. The 4-Methylumbelliferone (4-MU) release amount was determined by microplate reader at the excitation wavelength of 320 nm and the emission wavelength of 450 nm.

For free enzyme activity measurement: 100 μL of 4-MUO solution, 50 μL of phosphate buffer, and 50 μL of PL solution (10 mg/mL) were added to the centrifuge tube. After incubating the reaction mixture for 10 min at a specific temperature, the process was terminated at 100 °C.

For immobilized enzyme activity measurement: the centrifuge tube was filled with 100 μL of 4-MUO solution and 100 μL of phosphate buffer solution. The CFP/CS/GA/PL was added to the obtained solution above. The enzymatic process was stopped by removing CFP/CS/GA/PL with tweezers after 10 min of incubation at a particular temperature.

2.6. Performance of immobilized PL

By measuring the amount of product from different immobilized PL produced in the same manner, batch-to-batch reproducibility was examined. After 10 enzymatic reactions, the residual activity of immobilized PL was determined, indicating its reusability. After being removed from the reaction mixture, immobilized PL was cleaned three times with 30 mM phosphate buffer (pH 6.0) for subsequent run. During 30 days of storage, the storage stability was assessed by comparing the activity changes of free and immobilized PL.

2.7. Enzyme kinetic and inhibition kinetic study

The method of enzyme kinetic and inhibition kinetic study is based on previous literature reports with slight modifications [13]. The

affinity between enzyme and substrate can be represented by the Michaelis-Menten constant (*Km*), with the lower the *Km* value indicating higher affinity. *Km* of free and immobilized enzyme was calculated using the Michaelis-Menten equation (1):

$$1/V = K_m/V_{max} \bullet 1/[S] + 1/V_{max} \quad (1)$$

Where [*S*] means the substrate concentration, and *V* and *Vmax* represent the initial rate and the maximum rate of the enzymatic reaction. *Km* of immobilized and free PL was determined by measuring PL activity with 4-MUO concentrations ranging from 0.8 mM to 20 mM. The measurement was performed twice, and the amount of 4-MU represents the initial enzyme reaction rate.

Using Orlistat as a model inhibitor, the inhibition kinetics of immobilized PL was studied and the reliability of assay method was evaluated. To determine the half-maximal inhibitory concentration (IC_{50}), the inhibition curve was constructed using the logarithm of Orlistat concentration and inhibition rate. Equation (2) was used to calculate the inhibition rate.

$$\text{Inhibition}\% = \left(1 - x/Blank\right) \times 100\% \quad (2)$$

where *blank* and *x* are the 4-MU release amount without and with inhibitor.

2.8. Screening of PL inhibitors in NPs and PL ligands in black tea extract

To screen inhibitors from 26 NPs using the immobilized PL, an enzymatic reaction was conducted with 5 mg/mL of NPs extract. 100 μL of 4-MUO solution was mixed with 100 μL of NPs extract, followed by the addition of CFP/CS/GA/PL and incubation for 10 min.

Ligand screening was performed using previously reported methods. Briefly, 400 μL of 10 mg/mL black tea extract diluted in pH 8.0 phosphate buffer (30 mM) was incubated at 45 °C for 30 min with three discs of CFP/CS/GA/PL. The CFP discs were removed from the incubation solution and rinsed three times with 400 μL of phosphate buffer. Subsequently, the CFP discs were immersed for 10 min in a 400 μL 50 % methanol solution. This procedure was repeated three times. The dissociation solution was mixed, concentrated and dried using a vacuum centrifugal concentrator. The residue was redissolved in 100 μL 50 % methanol for UHPLC-QTOF-MS/MS analysis. Blank CFP/CS/GA was utilized as a control to exclude nonspecific binding. Equation (3) was used to calculate compound's binding rate. Compounds with binding rate of greater than 50 % are considered as potential inhibitors.

$$\text{Binding rate}\% = (\Delta Ae - \Delta Ac)/\Delta Ae \times 100\% \quad (3)$$

Where *ΔAe* is the amount of ligand captured in the experimental group, and *ΔAc* is the amount of ligand captured in the control group.

2.9. Molecular docking

Computer-simulated molecular docking technology through AutoDock 4.2.6 and AutoDock Tools 1.5.6 software was carried out to investigate the interaction of PL and ligands [14]. All compounds docked with PL were provided with 3D structures by PubChem (https://pubchem.ncbi.nlm.nih.gov/). Ligands were treated for added hydrogen atoms and charges, and torsional bonds were checked to minimize energy. The three-dimensional (3D) structure of the PL (PDB ID: 1ETH) was downloaded from Protein Data Bank (http://www.rcsb.org/pdb/home/home.do). The protein structures was then repaired by removing unnecessary hydrogen atoms and crystal water molecules, adding polar hydrogens and adding Kollman charges. The size of the grid was 126 Å × 126 Å × 126 Å and the grid centers were 64.0, 29.151 and 125.424. The docking results were visualized using PyMOL and Discovery Studio 2019.

2.10. Fluorescence spectrometry

The method of fluorescence spectrometry is based on previous literature reports with slight modifications [15]. Various concentrations of inhibitor (0, 1, 2, 3, 4, 5, 6, 7, 8 μM) were successively added to the PL solution (5 mg/mL). The fluorescence quenching reaction was examined using a F-7100 fluorescence spectrometer (Hitachi, Japan) at two different temperatures (298 and 310 K). The excitation wavelength of fluorescence spectrophotometer was set at 280 nm, the emission wavelength was set at 290–500 nm, and the slit width was set at 5 nm for the determination. The Stern-Volmer equation was used to determine the type of quenching of PL by the inhibitor.

$$F_0/F = 1 + K_{sv}[Q] = 1 + K_q\tau_0[Q] \quad (4)$$

Where *F* and F_0 are the maximum fluorescence intensity of PL with and without the addition of inhibitor, respectively; [*Q*] is the concentration of inhibitor, mol/L; τ_0 is the average fluorescence molecule lifetime in the absence of inhibitor (1×10^{-8}s); K_q is the bimolecular quenching constant, L/(mol·s); K_{sv} represents the Stern-Volmer quenching constant, L/mol.

The *F* and F_0 obtained at different temperatures were brought into the following equation and plotted with lg[*Q*] as the horizontal coordinate and lg[*(F₀–F)/F*] as the vertical coordinate to calculate the binding constants (K_a) and the number of binding sites (*n*) of inhibitor with PL.

$$\lg(F_0 - F)/F = \lg K_a + n \lg[Q] \quad (5)$$

The K_a value and the corresponding temperature (*T*) were fitted by the van't Hoff equation and the Gibbs–Helmholtz equation to determine the enthalpy change (*ΔH*) and entropy change (*ΔS*).

$$\ln K_a = -\Delta H/RT + \Delta S/R \quad (6)$$

$$\Delta G = \Delta H - T\Delta S \quad (7)$$

Where R is the gas constant (8.314), J/(mol·K); *T* is the absolute temperature.

2.11. Network pharmacology

2.11.1. Intersection of active compounds and obesity-related targets

We searched the GeneCards (https://www.genecards.org/) with "obesity" as the keyword. Epigallocatechin gallate, theaflavin-3-gallate and theaflavin-3,3′-digallate related targets were searched using Drugbank (www.drugbank.ca/) and SwissTargetPrediction (http://www.swisstargetprediction.ch/). The proteins of active compound candidate targets and obesity-related genes were uploaded to Venny software to obtain their intersection.

2.11.2. Construction of the protein-protein interaction (PPI) network

Intersection genes were imported into the String database (https://string-db.org/), with the target species set to *Homo sapiens for* PPI analysis. Import the analysis results into Cytoscape 3.7.1 (https://cytoscape.org/) and use the "Network Analyzer" plugin to rebuild and analyze the PPI network.

2.11.3. Gene ontology (GO) and kyoto encyclopedia of genes and genomes (KEGG) enrichment analysis

GO and KEGG enrichment analyses of potential targets were performed using DAVID (https://david.ncifcrf.gov/). The "Bioinformatics" online platform (www.bioinformatics.com.cn) was used to visualize results.

2.12. Statistical analysis

The data analysis and statistics were conducted by using Origin 2018 software (OriginLab, Northampton, MA, USA).

3. Results and discussions

3.1. Optimization of immobilization conditions

3.1.1. GA concentration

The effect of GA concentration ranging from 2.5 % to 15.0 % on the activity of immobilized PL was studied. As depicted in Fig. S1A, the catalytic activity of immobilized PL increased as the concentration of GA increasing from 2.5 % to 10.0 %. A rise in GA concentration may provide additional binding sites, leading to an increase in the number of enzymes immobilized on CFP. However, as the concentration of GA climbed to 15.0 %, the relative activity dropped, possibly due to excessive cross-linking resulting in reduced enzyme flexibility [10]. Additionally, widespread interaction with GA might result in conformational changes in enzyme proteins [16]. Given all that, GA concentration of 10.0 % was selected.

3.1.2. Crosslinking time

The crosslinking time determines the amount of GA modified on the CFP, thus affecting the immobilized amount of PL. At the crosslinking time of 3.0–7.0 h, the activity change of immobilized PL was studied. As shown in Fig. S1B, the relative activity increased as the increasing crosslinking time and reached a peak at 5.0 h, after which it decreased significantly. This decrease could be attributed to the longer crosslinking time causing overcrowding of the enzyme molecules on the CFP, thereby reducing the exposure of active sites [17]. Therefore, 5.0 h was chosen as the cross-linking time for the immobilized PL.

3.1.3. Enzyme concentration

The amount of enzyme attached to the carrier is directly influenced by the enzyme concentration. In the range of 5.0–15.0 mg/mL enzyme concentration, the activity change of immobilized PL was examined. According to Fig. S1C, enzyme activity increased as the PL concentration increased and reached a maximum at 10.0 mg/mL, demonstrating that the enzyme load had reached saturation. However, with the further increase of PL concentration, the hindrance on mass transfer caused by the crowding space becomes the main reason for the reduced enzyme activity [18]. Thus, a 10.0 mg/mL enzyme concentration was selected.

3.1.4. Immobilization pH

The pH level during immobilization has an effect on the forms of functional groups. The effect of immobilization pH values ranging from 5.0 to 9.0 on enzyme activity was studied. The relative activity peaked at pH 6.0, as indicated in Fig. S1D. Under acidic conditions, enzyme molecules would protonate, which is less conducive to the Schiff base reaction between the amino group of the enzyme and the aldehyde group of GA. Therefore, catalytic activity was decreased at pH 5.0. However, as the pH further increased to 9.0, the catalytic activity of immobilized PL decreased because excessively high pH renders the enzyme inactive [19]. Thus, the immobilization pH of 6.0 was chosen.

3.1.5. Immobilization time

The immobilized quantity of enzyme and the binding extent of the enzyme to the carrier are affected by the immobilization time. The influence of immobilization time ranging from 2.0 h to 10.0 h on enzyme activity was investigated. As depicted in Fig. S1E, the relative activity peaked at 6.0 h and then declined with increasing immobilization time. This is because the amount of immobilized enzyme increased with increasing immobilization time, but the overcrowded enzyme will gather, thus covering the active site and decreasing catalytic activity [20]. Therefore, the immobilization time was chosen as 6.0 h.

3.2. Influences of reaction conditions on enzyme activity

At a reaction temperature range of 30–80 °C, the catalytic activity of immobilized and free PL was compared. Fig. S2A demonstrates that the highest catalytic rates of both free and immobilized enzymes occurred at 50 °C. Moreover, the immobilized enzyme was able to maintain high relative activity at a variety of temperatures. Compared to the free reaction, the immobilized PL exhibited greater temperature endurance in the investigated temperature range. This is likely due to the multipoint covalent linking between PL and CFP, which makes the conformation of the enzyme protein more stable, thus making it more rigid in order to preserve its active structure [21]. Therefore, the enzymatic reaction temperature was set at 50 °C.

The effect of reaction pH between 5.0 and 10.0 on the relative activity of free and immobilized PL was depicted in Fig. S2B. The relative activities of both the immobilized and the free PL had an initial tendency to increase, followed by a decrease as pH increased, and both reached the highest value at pH 8.0. The enzyme activity of immobilized PL was greater than that of free protein in a wider pH range, suggesting that immobilized PL is more resistant to extreme pH values. This may be because immobilization makes the structure and conformation of the enzyme protein more stable and less susceptible to destruction by alkali and acid [22]. Thus, the pH of the reaction was set at 8.0.

3.3. Performance of immobilized PL

Three different batches of immobilized PL were used to assess reproducibility. The relative standard deviation of the amount of released product is 3.06 %, which illustrates the stability and dependability of the immobilization method.

As shown in Fig. S3A, the immobilized PL demonstrated excellent operational stability and retained 73.41 % of its initial activity after 10 consecutive reactions. The immobilized PL provided more economic advantages, better reusability, and lower operational expenses than the free enzyme, which can only be used once.

Another important consideration in practice is the storage stability of immobilized PL. As shown in Fig. S3B, the immobilized and free PL retained 72.81 % and 35.56 % residual activity, respectively, after 30 days of storage at 4 °C, indicating that the immobilized PL exhibited good storage stability.

3.4. Enzyme kinetics and inhibition kinetics study

As shown in Fig. S4, the Lineweaver-Burk plots of immobilized and free PL were $1/v = (1.18111 \pm 0.0556)\cdot(1/[S]) + (0.28657 \pm 0.0112)$ and $1/v = (0.55648 \pm 0.03853)\cdot(1/[S]) + (0.07739 \pm 0.00717)$. The *Km* values obtained from the intercept of the abscissa are 4.12 mM and 7.19 mM, respectively. Immobilized PL had a lower *Km*, indicating that its affinity for 4-MUO was stronger than that of free PL, and that it was more catalytically active. This may be a result of the greater accessibility of the substrate to the active site of the immobilized enzyme and a milder diffusion barrier effect compared to the free enzyme [23].

Fig. S5 depicts the double reciprocal plots generated at different Orlistat concentrations (10 μM, 30 μM, 50 μM). As the concentration of Orlistat increases, the vertical axis intercept ($1/Vmax$) increases, while the horizontal axis intercept (−1 /Km) remains unchanged. It can be concluded that Orlistat is a non-competitive inhibitor, which is consistent with previous reports [24]. As shown in Fig. S6, the inhibition constant Ki is 21.80 μM by secondary plot method, which is consistent with the literature [25]. The IC_{50} can be used to further evaluate the inhibitor's capacity. The dose-inhibition curve plotted by varying Orlistat concentrations is depicted in Fig. S7. The calculated IC_{50} value is 15.62 μM, which corresponds to prior results [26].

3.5. Screening of PL inhibitors in NPs

26 NPs were screened by CFP/CS/GA/PL, and the inhibition rate for each NP was determined using equation (2) and displayed in Table 1. Among the 26 NPs evaluated, black tea, kuding tea and longjing tea showed good inhibitory effects, with inhibition rates of 72.80 %, 63.39 % and 61.51 %, respectively. The results are consistent with the known benefits of tea on fat loss and obesity prevention [27], indicating that this approach could screen PL inhibitors reliably and rapidly. Consequently, black tea, with the highest inhibition rate, was selected for further exploration of compounds with PL bioactivity.

3.6. Capturing of PL ligands from black tea extract

The immobilized PL was used for capturing potential PL ligands from black tea extract. Comparing the peak areas of the two groups of compounds, as shown in Fig. 1, revealed that three compounds in the black tea extract exhibited strong binding affinities with binding rates greater than 50 %, suggesting that these compounds may possess potential PL bioactivity. By comparing known compounds isolated from black tea [28], these compounds were identified as epigallocatechin gallate, theaflavin-3-gallate and theaflavin-3,3′-digallate, as shown in Table 2. In fact, these three compounds have been reported to significantly inhibit PL activity [29]. In addition, theaflavins are the characteristic components of black tea [30], with theaflavin-3,3′-digallate having the highest content and biological activity [31]. The IC_{50} determined for theaflavin-3,3′-digallate was 2.63 μM, which was similar to the reported value [31]. These results emphasize the usefulness of immobilized PL, which has been successfully applied to screen potential inhibitors in black tea extract.

3.7. Molecular docking

The binding energy obtained from molecular docking of PL-epigallocatechin gallate, PL-theaflavin-3-gallate, and PL-theaflavin-3,3′-digallate systems were −9.1 kcal/mol, −9.3 kcal/mol, and −9.0 kcal/mol, respectively, This indicates that these three compounds have a good binding affinity with PL. Epigallocatechin gallate can form two hydrogen bonds with His152 and Tyr115. Discovery Studio 2019 indicated obvious electrostatic interactions between the benzene ring of epigallocatechin gallate with the amino acid residue His264 of PL, and hydrophobic interaction between epigallocatechin gallate with the amino acid residue Ala261、Phe78、Phe216、Leu265 of PL. Amino acid residue Arg 257、Pro 181、 Leu 154、 Glu180 interacted with epigallocatechin gallate to form van der Waals forces (Fig. 2A). The hydroxyl group of gallate theaflavin and the carbonyl group of gallate theaflavin can form hydrogen bonds with Asp258 and Asn263, respectively. Amino acid residue Cys262 interacted with theaflavin-3-gallate to form van der Waals force (Fig. 2B). Theaflavin-3,3′-digallate could form seven hydrogen bonds with Gln307、Asp279、Asn424、Cys305、Glu303、Asp425 and Arg423. Meanwhile, shown as Fig. 2C, discovery Studio 2019 showed the obvious electrostatic interactions between the benzene ring of theaflavin-3,3′-digallate and the amino acid residue Glu392 of PL. Amino acid residue Gly280、Cys300、Trp339、Ala282、Pro306、Phe315、Asp395 and Gly394 interacted with theaflavin-3,3′-digallate to form van der Waals forces.

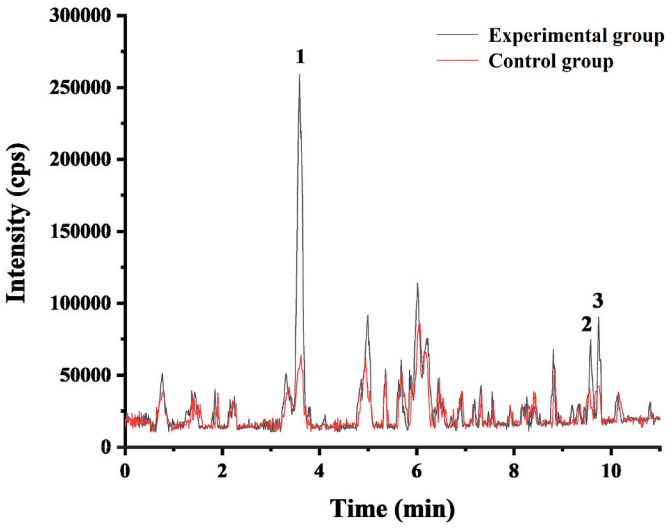

Fig. 1. Screening results of black tea extract by ligand capturing.

3.8. Fluorescence quenching of PL by theaflavin-3,3′-digallate

In order to understand the binding properties of theaflavin-3,3′-digallate with PL, the fluorescence quenching of PL by theaflavin-3,3′-digallate at two different temperatures (298 K and 310 K) was determined, as shown in Fig. S8. The F_0/F values at different temperatures showed a good linear relationship with the quencher concentration, as shown in Fig. S9, indicating a single quenching mode. As shown in Table 3, the values of K_{sv} decreased with the increase of temperature. Furthermore, the values of K_q were greater than the maximum diffusive collisional quenching rate constant (2×10^{10} L/(mol·s)), which indicated that theaflavin-3,3′-digallate-treated PL fluorescence quenching belonged to static quenching type.

The binding constant (K_a) and the number of binding sites (n) were calculated based on the double-logarithm regression plot, which are listed in Fig. S10 and Table 3. The K_a value for the binding of theaflavin-3,3′-bis-gallate to PL decreased with increasing temperature, indicating that the complex formed by the two is less stable at higher temperatures. In addition, the n value of approximately 1 indicates that theaflavin-3,3′-digallate has only one binding site on the PL (Table 3).

The values of the thermodynamic parameters can be obtained from the thermodynamic equations to determine the type of force that theaflavin-3,3′-digallate has with PL, and the specific values are shown in Table 3. The ΔG values at different temperatures suggest that the binding process of PL to theaflavin-3,3′-digallate is spontaneous. ΔH

Table 1
Inhibitory effects of 26 NP extracts on immobilized PL.

NPs	Inhibition (%)	NPs	Inhibition (%)	NPs	Inhibition (%)
Black Tea	72.80 ± 1.54	Radix isatidis	54.39 ± 0.92	Radix angelicae sinensis	42.89 ± 4.03
Kuding Tea	63.39 ± 0.57	*Lycopodium japonicum*	52.93 ± 1.33	*Lycium barbarum*	36.82 ± 5.03
Longjing Tea	61.51 ± 2.17	*Radix ginseng rubra*	52.30 ± 5.26	*Moringa oleifera*	33.47 ± 3.14
Lotus Seed	60.67 ± 5.32	Tangerine Peel	51.46 ± 0.86	Grape	24.69 ± 4.44
Hawthorn	60.67 ± 5.32	Coffee	51.05 ± 5.13	Raisin	21.76 ± 4.81
Schisandra chinensis	60.25 ± 2.11	Chrysanthemum	50.84 ± 2.98	Phryma leptostachya	21.13 ± 3.45
Honeysuckle	59.62 ± 2.59	*Lilium brownii*	48.54 ± 4.07	Ginseng	8.16 ± 0.68
Spatholobus suberectus	57.74 ± 1.98	*Radix astragali*	45.40 ± 1.92	Ginger	4.39 ± 1.09
Biluochun Tea	56.90 ± 3.88	*Zingiber mioga*	44.14 ± 5.62		

Values are showed as the mean ± SD (n = 3).

Table 2
UHPLC-QTOF-MS/MS identification of the PL ligands captured in black tea extract.

Peak	Compound	Binding rate (%)	Formula	tR (min)	$[M-H]^+$	Fragments
1	Epigallocatechin gallate	80.36	$C_{22}H_{18}O_{11}$	3.50	457.0790	125.0235, 169.0137, 161.0236, 305.0682
2	Theaflavin-3-gallate	53.27	$C_{36}H_{28}O_{16}$	9.50	715.1331	125.0235, 169.0137, 321.078, 269.0443, 281.0466, 137.0235, 241.0517, 253.0522, 563.1191
3	Theaflavin-3,3′-digallate	64.97	$C_{43}H_{32}O_{20}$	9.64	867.1440	867.1440, 169.0137, 125.0235, 389.0676, 401.0671, 527.1024, 697.1218, 137.0237, 559.0895

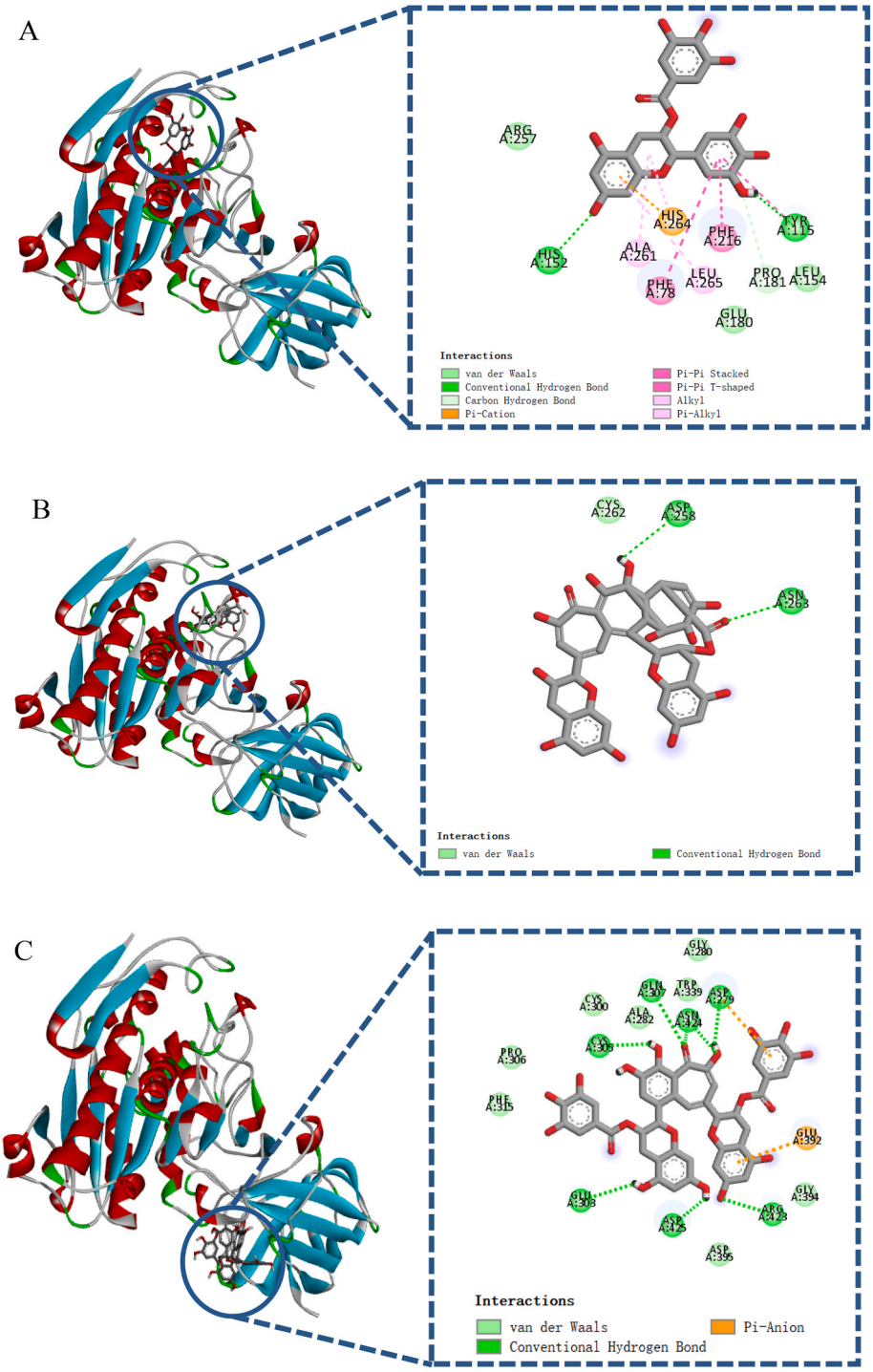

Fig. 2. The binding modes with interaction effects of epigallocatechin gallate (A), theaflavin-3-gallate (B), theaflavin-3,3′-digallate (C) to PL.

Table 3
The quenching rate constants (K_{sv}), correlation coefficients (K_q), correlation coefficients (R_1), apparent binding constant (K_a), binding site number (n), correlation coefficients (R_2), and thermodynamic parameters (ΔH, ΔS, and ΔG) of PL-theaflavin-3,3′-digallate complex.

Temperature (K)	R_1^2	K_{sv} (L/mol)	K_q(L/(mol·s))	R_2^2	K_a (L/mol)	n	ΔH (KJ/mol)	ΔS (J/mol/K)	ΔG (KJ/mol)
298	0.9882	8.105×10^4	7.842×10^{12}	0.9808	8.1410×10^3	0.8483	−18.72	12.04	−22.31
310	0.9793	4.963×10^4	4.903×10^{12}	0.9749	5.3079×10^3	0.8111		10.09	−22.11

values indicate that the combination of the two is an exothermic process. The positive ΔS and negative ΔH values indicate that the interaction between PL and theaflavin-3,3′-digallate was electrostatic interaction (Table 3). This result is consistent with the results of molecular docking.

3.9. Network pharmacology

The advancement of bioinformatics has rendered network pharmacology a viable and efficient tool for illuminating the potential biological role of small molecules in chemoprophylaxis of numerous chronic diseases [12]. By combining data from publicly accessible databases, the potential targets, associated networks and signaling pathways of three active compounds in black tea to ameliorate obesity were predicted.

3.9.1. Candidate targets of active compounds in obesity treatment

A median screening of obesity related targets obtained from GeneCards yielded 1266 pathological targets. After integrating the targets of epigallocatechin gallate, theaflavin-3-gallate and theaflavin-3,3′-digallate, obtained from DrugBank and SwissTargetPrediction, a total of 1498 targets were obtained. Fig. S11 illustrated 244 intersection targets between the active compounds in black tea and the obesity, including the PNLIP gene encoding PL.

3.9.2. PPI network construction and key target discovery

As seen in Fig. S12A, the PPI network contains 241 nodes (proteins) and 1299 edges (signifying the relationships between proteins). The first 15 targets in PPI network were selected by screening the degree, betweenness and closeness. These core targets are AKT1, GAPDH, VEGFA, PPARG, TP53, MAPK3, STAT3, SRC, CASP3, MYC, HSP90AA1, MMP9, HIF1A, PTEN and PPARA, as shown in Fig. S12B. Among them, PPARG is an upstream gene that regulates PNLIP.

3.9.3. GO and KEGG enrichment analysis

GO and KEGG enrichment analysis revealed that three active compounds in black tea were involved in 356 biological processes (BPs), 51 cellular components (CCs), 96 molecular functions (MFs), and 147 pathways for the treatment of obesity ($P < 0.01$). The top 20 entries for BPs, MFs, and CCs are shown in Fig. 3A–C. GO enrichment analysis showed that three active compounds mainly affected the biological processes of response to drug, signal transduction, response to xenobiotic stimulus, response to lipopolysaccharide and aging to exert their therapeutic effect on obesity by reacting on extracellular region, extracellular space, plasma membrane, cytoplasm, mitochondrion and other cellular components. The effects on molecular functions mainly included enzyme binding, RNA polymerase II transcription factor activity, ligand-activated sequence-specific DNA binding, identical protein binding, zinc ion binding and serine-type endopeptidase activity.

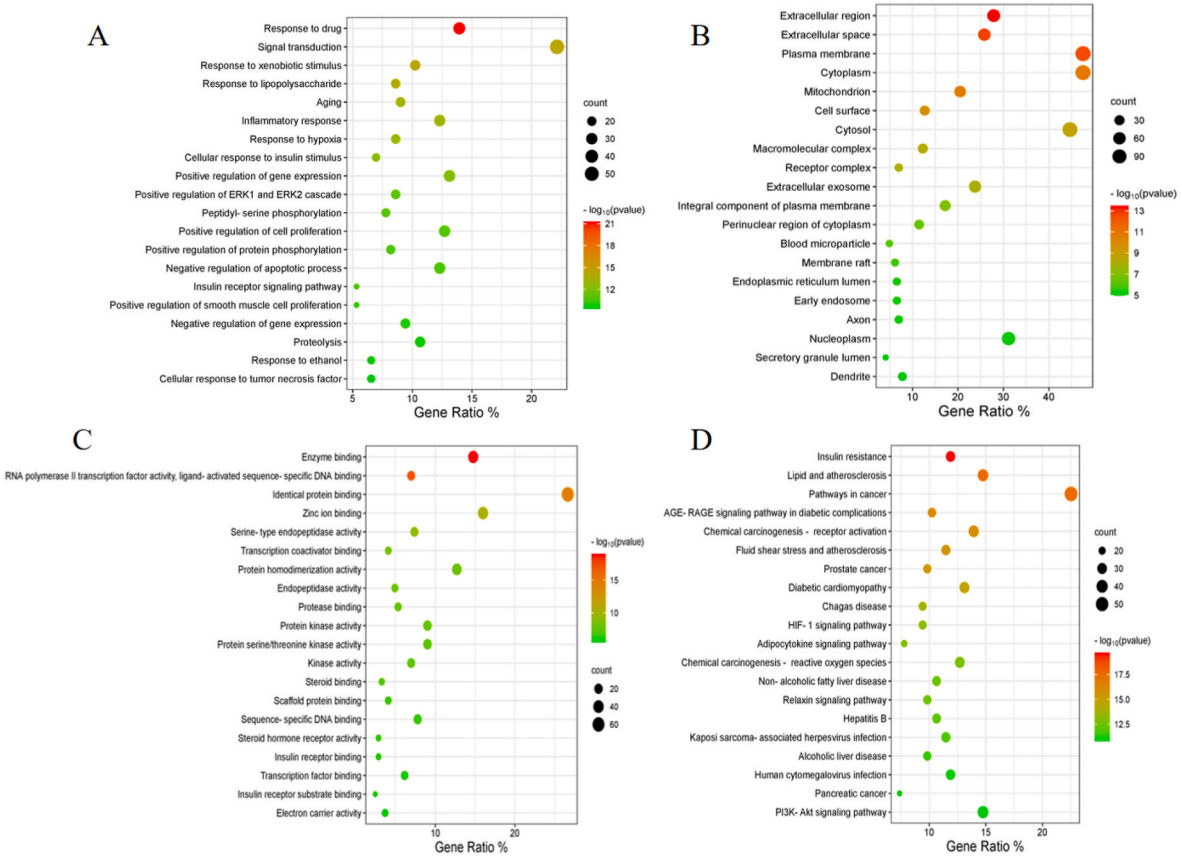

Fig. 3. Bubble diagram of GO and KEGG analysis results. BPs (A), CCs (B), MFs (C) and KEGG (D).

The top 20 signaling pathways according to KEGG enrichment analysis are shown in Fig. 3D. Insulin resistance is the most significantly enriched pathway, and it has been reported to increase PL activity [32]. Insulin resistance can result in non-alcoholic fatty liver disease, which may be related to the increased content of free fatty acids in the liver caused by PL, allowing more fat to accumulate in the liver [33]. In addition, tumor infiltration of pancreatic tissue in pancreatic cancer might result in elevated PL levels, which can affect lipid absorption [34]. The KEGG results indicated that insulin resistance, non-alcoholic fatty liver disease [35] and pancreatic cancer can be considered as important signaling pathways mediated by three compounds that regulate obesity.

4. Conclusions

In this study, CS was used as an amino modifier, while GA was used as a crosslinking agent to immobilize PL on CFP through the Schiff base reaction. The results proved the stability and reliability of the immobilized method, and the CFP/CS/GA/PL demonstrated excellent temperature and pH tolerance, storage stability, reproducibility and reusability. Its immediate separation from the reaction mixture simplifies subsequent kinetic studies and inhibitor screening, making the reuse of immobilized enzyme more feasible. In addition, a ligand capture strategy of immobilized PL coupled with UHPLC-QTOF-MS/MS was established and three compounds with PL inhibition were screened from black tea extract. Molecular docking results showed that each compound bound well and stably to the binding pocket of PL. Both molecular docking and fluorescence quenching experiments demonstrated binding between theaflavin-3,3′-digallate and PL by electrostatic interactions. These results imply that this technique provides a convenient and feasible option for rapid and effective screening of PL inhibitors from natural products and other complex systems. Moreover, network pharmacology has established a theoretical foundation for future studies on the anti-obesity effects of black tea by revealing the molecular mechanisms of three active compounds in black tea in chemoprevention of obesity.

CRediT authorship contribution statement

Guangxuan Chen: Writing – original draft, Methodology, Investigation. **Huicong Yuan:** Software, Visualization, Writing – review & editing. **Lumei Zhang:** Writing – original draft, Visualization, Software. **Jingran Zhang:** Resources. **Kefeng Li:** Resources. **Xu Wang:** Writing – review & editing, Supervision.

Declaration of competing interest

The authors declare that they have no known competing financial interests or personal relationships that could have appeared to influence the work reported in this paper.

Data availability

Data will be made available on request.

Acknowledgements

This work was supported by the Open Project Program of State Key Laboratory of Food Nutrition and Safety (NO. SKLFNS-KF-201820).

Appendix B. Supplementary data

Supplementary data to this article can be found online at https://doi.org/10.1016/j.talanta.2024.126750.

References

[1] L.-J. Ma, X.-D. Hou, X.-Y. Qin, R.-J. He, H.-N. Yu, Q. Hu, X.-Q. Guan, S.-N. Jia, J. Hou, T. Lei, G.-B. Ge, Discovery of human pancreatic lipase inhibitors from root of Rhodiola crenulata via integrating bioactivity-guided fractionation, chemical profiling and biochemical assay, Journal of Pharmaceutical Analysis 12 (4) (2022) 683–691.
[2] K.L. Canning, R.E. Brown, V.K. Jamnik, J.L. Kuk, Relationship between obesity and obesity-related morbidities weakens with aging, The journals of gerontology. Series A, Biological sciences and medical sciences 69 (1) (2014) 87–92.
[3] L. Rajan, D. Palaniswamy, S.K. Mohankumar, Targeting obesity with plant-derived pancreatic lipase inhibitors: a comprehensive review, Pharmacol. Res. 155 (2020) 104681.
[4] E. Kato, A. Tsuruma, A. Amishima, H. Satoh, Proteinous pancreatic lipase inhibitor is responsible for the antiobesity effect of young barley (Hordeum vulgare L.) leaf extract, Bioscience, biotechnology, and biochemistry 85 (8) (2021) 1885–1889.
[5] T.D. Filippatos, C.S. Derdemezis, I.F. Gazi, E.S. Nakou, D.P. Mikhailidis, M.S. Elisaf, Orlistat-associated adverse effects and drug interactions: a critical review, Drug Saf. 31 (1) (2008) 53–65.
[6] H. Xu, J. Qu, J. Wang, K. Han, Q. Li, W. Bi, R. Liu, Discovery of pulmonary fibrosis inhibitor targeting TGF-β RI in Polygonum cuspidatum by high resolution mass spectrometry with in silico strategy, J Pharm Anal 12 (6) (2022) 860–868.
[7] A.L. Hopkins, Network pharmacology: the next paradigm in drug discovery, Nat. Chem. Biol. 4 (11) (2008) 682–690.
[8] Y. Lu, Q. Luo, X. Jia, J.P. Tam, H. Yang, Y. Shen, X. Li, Multidisciplinary strategies to enhance therapeutic effects of flavonoids from Epimedii Folium: integration of herbal medicine, enzyme engineering, and nanotechnology, J Pharm Anal 13 (3) (2023) 239–254.
[9] Y. Yi, J. Hu, S. Ding, J. Mei, X. Wang, Y. Zhang, J. Chen, G. Ying, A preparation strategy for protein-oriented immobilized silica magnetic beads with Spy chemistry for ligand fishing, J Pharm Anal 12 (3) (2022) 415–423.
[10] D.M. Liu, J. Chen, Y.P. Shi, α-Glucosidase immobilization on chitosan-modified cellulose filter paper: preparation, property and application, Int. J. Biol. Macromol. 122 (2019) 298–305.
[11] J. Alftrén, T.J. Hobley, Covalent immobilization of β-glucosidase on magnetic particles for lignocellulose hydrolysis, Applied biochemistry and biotechnology 169 (7) (2013) 2076–2087.
[12] S.L. Glisan, K.A. Grove, N.H. Yennawar, J.D. Lambert, Inhibition of pancreatic lipase by black tea theaflavins: comparative enzymology and in silico modeling studies, Food Chem. 216 (2017) 296–300.
[13] Z. Xu, Q. Cao, A. Manyande, S. Xiong, H. Du, Analysis of the binding selectivity and inhibiting mechanism of chlorogenic acid isomers and their interaction with grass carp endogenous lipase using multi-spectroscopic, inhibition kinetics and modeling methods, Food Chem. 382 (2022) 132106.
[14] C. Zhang, Y. Ma, F. Gao, Y. Zhao, S. Cai, M. Pang, The free, esterified, and insoluble-bound phenolic profiles of Rhus chinensis Mill. fruits and their pancreatic lipase inhibitory activities with molecular docking analysis, J. Funct.Foods 40 (2018) 729–735.
[15] C. Wang, L. Chen, Y. Lu, J. Liu, R. Zhao, Y. Sun, B. Sun, W. Cuina, pH-Dependent complexation between β-lactoglobulin and lycopene: multi-spectroscopy, molecular docking and dynamic simulation study, Food Chem. 362 (2021) 130230.
[16] M.R. Ladole, J.S. Mevada, A.B. Pandit, Ultrasonic hyperactivation of cellulase immobilized on magnetic nanoparticles, Bioresour. Technol. 239 (2017) 117–126.
[17] F. López-Gallego, L. Betancor, A. Hidalgo, N. Alonso, G. Fernandez-Lorente, J. M. Guisan, R. Fernandez-Lafuente, Preparation of a robust biocatalyst of d-amino acid oxidase on sepabeads supports using the glutaraldehyde crosslinking method, Enzym. Microb. Technol. 37 (7) (2005) 750–756.
[18] S.K. Halder, C. Maity, A. Jana, K. Ghosh, A. Das, T. Paul, P.K.D. Mohapatra, B. R. Pati, K.C. Mondal, Chitinases biosynthesis by immobilized Aeromonas hydrophila SBK1 by prawn shells valorization and application of enzyme cocktail for fungal protoplast preparation, J. Biosci. Bioeng. 117 (2) (2014) 170–177.
[19] J. Jiang, Y. Yu, L. Wang, J. Li, J. Ling, Y. Li, G. Duan, Enzyme immobilized on polyamidoamine-coated magnetic microspheres for α-glucosidase inhibitors screening from Radix Paeoniae Rubra extracts accompanied with molecular modeling, Talanta 195 (2019) 127–136.
[20] H.H. Zhao, Y.Q. Liu, J. Chen, Screening acetylcholinesterase inhibitors from traditional Chinese medicines by paper-immobilized enzyme combined with capillary electrophoresis analysis, J. Pharm. Biomed. Anal. 190 (2020) 113547.
[21] G. Karageorgis, S. Warriner, A. Nelson, Efficient discovery of bioactive scaffolds by activity-directed synthesis, Nat. Chem. 6 (10) (2014) 872–876.
[22] T. Li, S. Li, N. Wang, L. Tain, Immobilization and stabilization of pectinase by multipoint attachment onto an activated agar-gel support, Food Chem. 109 (4) (2008) 703–708.
[23] L. Donato, C. Algieri, A. Rizzi, L. Giorno, Kinetic study of tyrosinase immobilized on polymeric membrane, J. Membr. Sci. 454 (2014) 346–350.
[24] J. Feng, S. Yu, J. Li, T. Mo, P. Li, Enhancement of the catalytic activity and stability of immobilized aminoacylase using modified magnetic Fe3O4 nanoparticles, Chem. Eng. J. 286 (2016) 216–222.
[25] C. Fu, Y. Jiang, J. Guo, Z. Su, Natural products with anti-obesity effects and different mechanisms of action, J. Agric. Food Chem. 64 (51) (2016) 9571–9585.
[26] J. Liu, R.T. Ma, Y.P. Shi, An immobilization enzyme for screening lipase inhibitors from Tibetan medicines, Journal of chromatography. A 1615 (2020) 460711.
[27] J. Liu, H.X. Zhang, Y.P. Shi, Lipase immobilization on magnetic cellulose microspheres for rapid screening inhibitors from traditional herbal medicines, Talanta 231 (2021) 122374.

[28] Z. Zhang, C. Liu, W. Fang, Q. Tang, L. Zhan, Y. Shi, M. Tang, Z. Liu, S. Zhang, A. Liu, Research progress on the lipid-lowering and weight loss effects of tea and the mechanism of its functional components, J. Nutr. Biochem. 112 (2023) 109210.

[29] N. Chen, B. Han, X. Fan, F. Cai, F. Ren, M. Xu, J. Zhong, Y. Zhang, D. Ren, L. Yi, Uncovering the antioxidant characteristics of black tea by coupling in vitro free radical scavenging assay with UHPLC-HRMS analysis, J. Chromatogr., B: Anal. Technol. Biomed. Life Sci. 1145 (2020) 122092.

[30] J. Ju, G. Lu, J.D. Lambert, C.S. Yang, Inhibition of carcinogenesis by tea constituents, Semin. Cancer Biol. 17 (5) (2007) 395–402.

[31] N. Yuda, M. Tanaka, M. Suzuki, Y. Asano, H. Ochi, K. Iwatsuki, Polyphenols extracted from black tea (Camellia sinensis) residue by hot-compressed water and their inhibitory effect on pancreatic lipase in vitro, Journal of food science 77 (12) (2012) H254–H261.

[32] D. Shi, L. Liu, H. Li, D. Pan, X. Yao, W. Xiao, X. Yao, Y. Yu, Identifying the molecular basis of Jinhong tablets against chronic superficial gastritis via chemical profile identification and symptom-guided network pharmacology analysis, J Pharm Anal 12 (1) (2022) 65–76.

[33] R.D. Duan, C. Erlanson-Albertsson, Pancreatic lipase and colipase activity increase in pancreatic acinar tissue of diabetic rats, Pancreas 4 (3) (1989) 329–334.

[34] R.H. Al Zarzour, M. Ahmad, M.Z. Asmawi, G. Kaur, M.A.A. Saeed, M.A. Al-Mansoub, S.A.M. Saghir, N.S. Usman, D.W. Al-Dulaimi, M.F. Yam, Phyllanthus niruri standardized extract alleviates the progression of non-alcoholic fatty liver disease and decreases atherosclerotic risk in sprague-dawley rats, Nutrients 9 (7) (2017).

[35] M. Stotz, D.A. Barth, J.M. Riedl, E. Asamer, E.V. Klocker, P. Kornprat, G. C. Hutterer, F. Prinz, K. Lackner, H. Stöger, A. Gerger, M. Pichler, The lipase/amylase ratio (LAR) in peripheral blood might represent a novel prognostic marker in patients with surgically resectable pancreatic cancer, Cancers 12 (7) (2020).